

## X-ray observation of micro-failures in granular piles approaching an avalanche

A. KABLA<sup>1</sup>, G. DEBRÉGEAS<sup>2</sup>, J.-M. DI MEGLIO<sup>1,3</sup> and T. J. SENDEN<sup>1</sup>

<sup>1</sup> *Department of Applied Mathematics, Research School of Physical Sciences and Engineering, The Australian National University - Canberra, Australia*

<sup>2</sup> *LFO-Collège de France, CNRS UMR 7125 - Paris, France*

<sup>3</sup> *MSC, CNRS, Université Paris 7 - Paris, France*

received 31 May 2005; accepted 8 July 2005

published online 10 August 2005

PACS. 45.70.Cc – Static sandpiles; granular compaction.

PACS. 45.70.Ht – Avalanches.

PACS. 81.05.Rm – Porous materials; granular materials.

**Abstract.** – An X-ray imaging technique is used to probe the stability of 3-dimensional granular packs in a slowly rotating drum. Well before the surface reaches the avalanche angle, we observe intermittent plastic events associated with collective rearrangements of the grains located in the vicinity of the free surface. The energy released by these discrete events grows as the system approaches the avalanche threshold. By testing various preparation methods, we show that the pre-avalanche dynamics is not solely controlled by the difference between the free surface inclination and the avalanche angle. As a consequence, the measure of the pre-avalanche dynamics is unlikely to serve as a tool for predicting macroscopic avalanches.

When a granular pack is submitted to a slowly varying stress its apparent response consists in intermittent bursts of plasticity during which large irreversible deformations take place [1,2]. Between these discrete events the system behaves as a rigid body. Formation of shear-bands in granular systems in triaxial tests [3], the jamming and unjamming of an hourglass [4] or sequences of avalanches down a sandy slope are common examples of this intermittent behavior. Because of its relevance to geophysics and the possibility of direct observations, the case of avalanches have been studied in great detail since the early work of Bagnold [5]. It was found that the intermittent regime occurs between two limiting angles of the heap surface: the repose and the avalanche angle which depend on the geometry as well as the characteristics of the material (shape and surface properties of the grains) [6]. Although the main features of the avalanche flow are rather well understood [7–9], one important question remains to date unsolved: what is the nature of the microscopic process by which the flow is triggered and later stopped during a single avalanche?

To address this question, several experimental and numerical studies have recently focused on micro-plasticity [10,11]. Indeed it appears that even in the absence of visible flow, any modification of the external force applied to a granular pack induces some micro-displacements which allow the system to mechanically adapt to the new constraints. By analogy with earthquakes, these events could be seen as precursors of the macroscopic failure of the pack. Although they dissipate only a small fraction of the energy as compared to the macroscopic avalanches, they could impact the stress distribution within the static pack therefore controlling its overall stability.

TABLE I – Different types of grains used in the experiments.  $\theta_a$  is defined as the average inclination angle of the surface in the avalanche regime. The size corresponds to the diameter for the spheres. The cylinder is  $2.2 \pm 0.2$  mm in height and diameter. Glassy carbon beads were obtained from Hochtemperatur-Werkstoffe GmbH, pasta was De Cecco Acini di pepe.

|     | Material | Shape    | Size   | $\theta_a$ |
|-----|----------|----------|--------|------------|
| I   | pasta    | cylinder | 2.2 mm | 30         |
| II  | carbon   | sphere   | 1.1 mm | 27         |
| III | carbon   | sphere   | 0.8 mm | 26         |
| IV  | carbon   | sphere   | 0.4 mm | 22         |

In the present work, we use an X-ray imaging technique to probe the energy and spatial characteristics of these precursors in 3D granular systems slowly tilted towards the avalanche angle. Experiments are done in a cylindrical acrylic drum 55 mm in diameter with a depth of 30 mm. The drum is half-filled with various types of grains, table I, and mounted with its rotation axis parallel to the X-ray beam. To prevent a bulk rotation of the sample, a disordered monolayer of grains is glued to the inner surface of the cylinder. The drum is co-axially mounted inside the central aperture of a precision rotation stage which allows for very smooth rotation and a maximal rotation speed of  $0.5^\circ\text{s}^{-1}$ . A micro-focus X-ray source is placed 230 cm from the drum and provides a weakly divergent beam which crosses the stage aperture, producing a radiograph on a scintillator-coupled CCD camera [12], fig. 1(a). For a monochromatic beam, the transmitted intensity of the incident beam at a position  $[x, z]$  reads:

$$I[x, z] = A(t) \cdot I_0[x, z] \cdot \mathbf{a}_c[x, z] \cdot \exp\left[-\frac{L_g[x, z]}{\lambda_g}\right]. \quad (1)$$

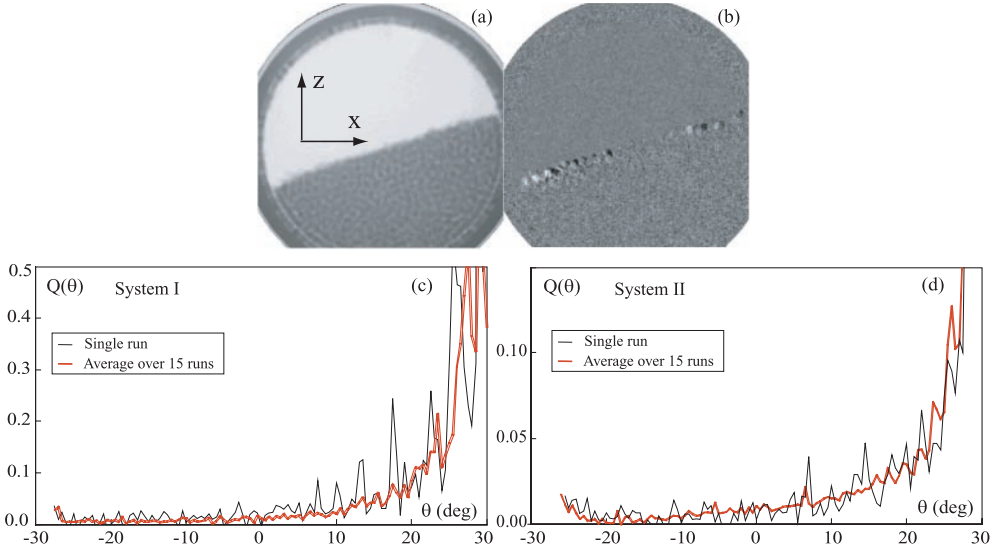


Fig. 1 – Measurement of the dynamics induced by a tilt increment for the system I (see table I): a) radiography of the drum; (b) picture presenting the variations of the crossed grains length  $\Delta L_g$ , at an angle  $20^\circ$ ; (c) and (d) measurements of the quadratic fluctuations as a function of the drum angular position  $\theta$ , respectively for the systems I and II. The thin black line corresponds to a single run, whereas the thick (red online) line shows the average over 15 runs. The data have been rescaled by the average of  $Q$  in the avalanche regime.

In this expression,  $A(t) \cdot \mathbf{I}_0[x, z]$  is the incident intensity map without sample ( $A(t)$  being the temporal fluctuations of the X-ray source intensity),  $\mathbf{a}_c[x, z]$  corresponds to the absorption of the empty container, and  $\lambda_g$  is the absorption length of the grain material. The total length of the grain material which projects through each position  $[x, z]$  on the drum is denoted,  $\mathbf{L}_g[x, z]$ .

To prepare the grain pack in a reproducible way, the drum is initially rotated  $360^\circ$  clockwise, leaving the pack surface at the avalanche angle  $-\theta_a$ . The drum is then rotated incrementally counter-clockwise. To probe whether a displacement has occurred over any given increment  $\delta\theta$  ( $0.5^\circ$ ), we use the following protocol: at  $\theta$  a radiograph of the pack is taken,  $\mathbf{I}_1[x, z](\theta)$ . The drum is further rotated to the angle  $\theta + \delta\theta$ , stopped for 5 s, then rotated back to  $\theta$  whereupon another radiograph  $\mathbf{I}_2[x, z](\theta)$  is taken. Finally, the drum rotates back to  $\theta + \delta\theta$  in preparation for the next increment. The change in  $\mathbf{L}_g[x, z]$ , by direct comparison between  $\mathbf{I}_1[x, z](\theta)$  and  $\mathbf{I}_2[x, z](\theta)$  quantitatively characterizes the pack dynamics:

$$\Delta\mathbf{L}_g(\theta) = \lambda_g \cdot \left[ \ln \left( \frac{\mathbf{I}_1(\theta)}{\mathbf{I}_2(\theta)} \right) - \left\langle \ln \left( \frac{\mathbf{I}_1(\theta)}{\mathbf{I}_2(\theta)} \right) \right\rangle_{[x,z]} \right]. \quad (2)$$

The average in eq. (2) corrects for temporal fluctuations in the X-ray source. A grey-scale representation of  $\Delta\mathbf{L}_g[x, z]$  is presented in fig. 1(b). This image demonstrates the existence of movements in the vicinity of the free surface. A closer examination reveals that these motions occur in the form of large clusters located near the free surface and moving over a fraction of the grain diameter.

Several measurements may be extracted from  $\Delta\mathbf{L}_g[x, z]$ . The quadratic average of  $\Delta\mathbf{L}_g(\theta)$ , denoted  $Q(\theta)$ , is a probe of the amplitude of small relative grain movements (a fraction of the grain size). Since this average also integrates the detector noise, we evaluate the contribution of the latter, denoted  $Q_0$ , by measuring the quadratic noise on successive pictures without rotation and taken under the same conditions as in the experiment. We subtract this value so that  $Q(\theta)$  only reflects grains motions:

$$Q(\theta) = \langle \Delta\mathbf{L}_g(\theta)^2 \rangle_{[x,z]} - Q_0. \quad (3)$$

This measurement appears to be very sensitive to relative grain displacements for the largest particles and thus provides a powerful tool for movement detection inside the 3D pack. However, for small grains, the contrast of the raw pictures vanishes which hampers us to perform such a measurement. In order to analyze the role of the grain size, we also extract, for the same system and protocol, the displacement  $(\Delta x_b, \Delta z_b)$  of the barycenter of the pack due to a tilt increment,  $\delta\theta$ :

$$(\Delta) x_b(\theta) \Delta z_b(\theta) = K \cdot \sum_{\{x,z\}} (x) z \Delta\mathbf{L}_g(\theta)[x, z]. \quad (4)$$

The sum is performed over all the positions  $[x, z]$ .  $K$  is chosen in order to express the distances  $\Delta x_b$  and  $\Delta z_b$  in drum radius unit. Though expressed as a length,  $\Delta z$  may also be interpreted as an energy variation. In contrast with the quadratic variations  $Q(\theta)$ , the measure of the pack barycenter displacement does not require a good contrast in the picture and is therefore suitable for small grains. Moreover, it allows a quantitative and direct comparison between different systems.

Figures 1(c) and (d) display the evolution of the quadratic fluctuations  $Q(\theta)$  for the largest particles (systems I and II in table I). The peaked events observed in the signal are a direct signature of an intermittent behavior in the micro-movements of the grains, well before the

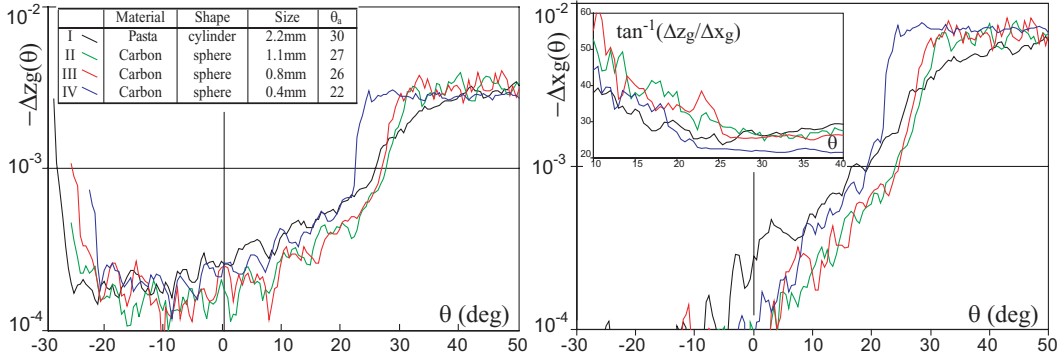


Fig. 2 – Normalized displacement of the pack barycenter for four different systems (color online). The length unit is set as the drum radius. I is the average over 15 runs, whereas II, III and IV are averaged over 25 runs. The inset describes the angular direction of the displacement.

surface reaches the avalanche angle. This observation is consistent with the 2D numerical simulations of Staron *et al.* [10]. The discrete events become detectable when the surface inclination approaches the horizontal. We thereafter observe a progressive increase of the magnitude of  $Q(\theta)$ , but no significant evolution of the intermittency frequency.

The displacements of the pack barycenter, on different systems, and with different grains sizes, are displayed in fig. 2. Three regimes may be distinguished. For  $-\theta_a < \theta < 0$ , we measure small values of  $\Delta z_b$ , whereas  $\Delta x_b$  remains insignificant. This indicates that a slight compaction occurs in the sample as expected when a granular system is mechanically perturbed. For  $0 < \theta < \theta_a$ , we observe a strong increase on both  $\Delta x_b$  and  $\Delta z_b$ . This evolution is associated with a progressive increase of the mean displacement direction, given by  $\tan^{-1}(\Delta x_b/\Delta z_b)$ , that eventually aligns with the free surface, fig. 2 inset. As the inclination reaches the avalanche angle  $\theta_a$ , we observe a sudden increase of the dynamics; beyond  $\theta_a$ , the flow occurs along the surface of the pack ( $\langle \tan^{-1}(\Delta x_b/\Delta z_b) \rangle = \theta_a$ ). The values of  $\Delta x_b$  and  $\Delta z_b$  simply correspond to the average grain flow necessary to compensate for the rotation of the drum.

Surprisingly, the measurement in the pre-avalanche regime seems to be independent of the grain type, and in particular of the grain size. This observation can be used to discriminate between two possible interpretations (see fig. 3): a) If the dynamics were due to a purely superficial effect, such as grains rolling, the thickness of the moving layer and the magnitude of the displacement would be controlled by the grain size. Hence, the average displacement

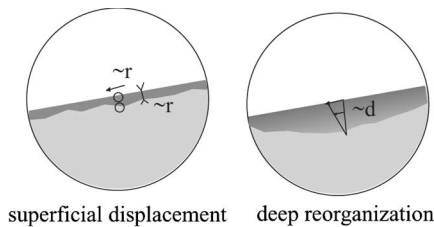


Fig. 3 – Illustration of the superficial and deep displacements. Case 1 (left): the displacement involves a superficial layer whose thickness scales with the grain size  $r$ , moving over a distance of the order of  $r$ . The barycentric displacement  $\Delta x$  then scales like  $r^2$ . Case 2 (right): the failure corresponds to a minute deformation of a layer whose thickness  $d$  is controlled by the drum size: in this case, the barycentric displacement is independent of the grain size.

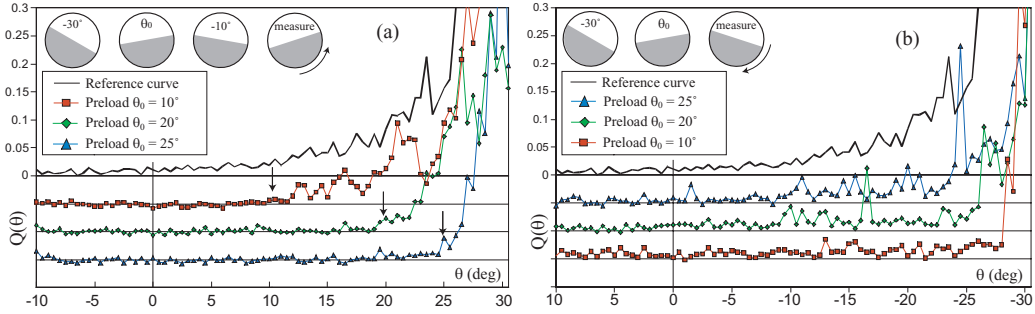


Fig. 4 – Role of the preparation (grain type I). (a) Effect of a pre-load up to an angle  $\theta_0$  on the dynamics. (b) Evaluation of the range of stability for different preparations. All the curves correspond to the average of four similar runs (except 15 for the reference curve). For a better visibility, graphs have been shifted.

in the pre-avalanche regime, expressed in units of drum radius, should scale as the square of the grain size. This is inconsistent with our observations. b) In contrast, the independence of the dynamics with grain size strongly suggests that the surface flow penetrates onto a depth  $d$  controlled by the drum geometry (diameter and/or thickness). The pre-avalanche regime thus corresponds to a macroscopic instability of the pack structure, though preferentially occurring in the vicinity of the surface.

In considering fig. 2, it is tempting to describe this instability as being controlled by the surface angle. To probe this hypothesis, we explore the effect of other parameters—such as the preparation—on the pre-avalanche dynamics. The following sequence of tilts is thus applied to the pack before starting the measurement: the pack is first rotated  $360^\circ$  clockwise, then slowly tilted backwards until the surface inclination reaches a prescribed angle  $\theta_0$ , and finally returned to a fixed value  $-10^\circ$ , fig. 4(a). From that point, the dynamics are recorded as the drum is rotated counter-clockwise using the usual protocol.

Figure 4(a) shows the evolution of the quadratic fluctuations  $Q(\theta)$  (eq. (3)) obtained for three different values of  $\theta_0$ , which are compared with the reference curve obtained with data from fig. 1 inset. Interestingly, the dynamics are, in all cases, negligible until the drum reaches the angle  $\theta_0$ . Beyond this value, the activity increases rapidly and shows similar features as in the non-pre-loaded sample. This result demonstrates that the pre-avalanche dynamics does not depend solely on the surface inclination. The absence of detectable plastic events from  $-10$  to  $\theta_0$  shows that the successive static configurations that the system experiences during a tilt experiment are stable over a large range of surface inclinations.

To probe in more detail the range of stability of each structure we perform a complementary experiment depicted in fig. 4(b). As previously shown, the system is rotated  $360^\circ$  clockwise, then tilted backwards to a prescribed angle  $\theta_0 < \theta_a$ . The dynamics is then recorded as the pack is rotated clockwise towards the avalanche angle. We observe that the threshold angle for which detectable motion occurs, and consequently the range of mechanical stability of the pack, depend on the preparation angle  $\theta_0$ . For  $\theta_0$  of the order of (or less than) 0, the pack remains stable until we reach  $-\theta_a$ . For larger values of  $\theta_0$ , the onset of internal dynamics occurs after a rotation of roughly  $30^\circ$ , regardless of  $\theta_0$ . These results indicate that each structural state of the pack is associated with a range of inclination angle within which it is mechanically stable (within the resolution of our measurements). The width of this stability range barely depends on the pre-charge angle, but the latter controls the value of its limiting angles.

From the observed pre-avalanche dynamics, one might be tempted to extrapolate informa-

tion about the triggering of macroscopic avalanche flows such as the avalanche angle. However, we find that grains with different avalanche angles exhibit quantitatively similar pre-avalanche behaviors, fig. 2. Moreover, we show that the preparation and history of the pile have a major impact on the statistics of the micro-events, but no significant effect on the avalanche angle [13]. As a consequence, the avalanche angle cannot be deduced from the measurement of the pre-avalanche dynamics alone, and it seems unlikely that the latter may serve as a tool for a robust prediction of the macroscopic avalanche.

These observations might reflect the fact that the two instabilities —pre-avalanche failures and avalanche triggering— are qualitatively different. The discrete micro-failures we have observed correspond to the mechanical destabilization of a static structure induced by an incremental tilt, and the energy released by each event is rapidly dissipated. The instability is thus only controlled by the static properties of the granular structure which reflect the preparation history of the pack. In contrast, the avalanche is a dynamical instability that primarily involves the dissipative properties of the material. A macroscopic avalanche is triggered when the pile cannot dissipate the inertial energy produced by any small failure [7, 8, 14].

We have presented here a new experimental technique suitable for the study of 3D confined granular dynamics, that allowed us to measure minute displacements of the structure. In contrast to other techniques (DWS [15] capacitive measurements [16]), our method allows for local and quantitative measurements of the deformation. We are currently using X-ray computerized tomography in order to obtain 3D information on these plastic events [17]. Beyond the displacement field, this method might enable us to directly probe the statistical properties of the contact network, which might control the plastic response of the material.

\* \* \*

We wish to thank T. ASTE for stimulating discussions, and T. SAWKINS for his helpful technical contributions.

## REFERENCES

- [1] NASUNO S., KUDROLLI A. and GOLLUB J. P., *Phys. Rev. Lett.*, **79** (1997) 949.
- [2] HOWELL D., BEHRINGER R. P. and VEJE C., *Phys. Rev. Lett.*, **82** (1999) 5241.
- [3] BESUELLE P., DESRUES J. and RAYNAUD S., *Int. J. Rock Mech. Mining Sci.*, **37** (2000) 1223.
- [4] BERTHO Y., GIORGIUTTI-DAUPHINÉ F. and HULIN J. P., *Phys. Fluids*, **15** (2003) 3358.
- [5] BAGNOLD R. A., *The Physics of Blown Sand and Desert Dunes* (Methuen, London) 1941.
- [6] DURAN J., *Sand, Powders and Grains: An Introduction to the Physics of Granular Materials* (Springer-Verlag, New York, Inc) 2000.
- [7] DAERR A. and DOUADY S., *Nature*, **399** (1999) 241.
- [8] RAJCHENBACH J., *Phys. Rev. Lett.*, **88** (2002) 14301.
- [9] GDR MIDI, *Eur. Phys. J. E*, **14** (2004) 341.
- [10] STARON L., VILOTTE J.-P. and RADJAI F., *Phys. Rev. Lett.*, **89** (2002) 204302.
- [11] DEBOEUF S., BERTIN E. M., LAJEUNESSE E. and DAUCHOT O., *Eur. Phys. J. B*, **36** (2003) 105.
- [12] SAKELLARIOU A., SAWKINS T. J., SENDEN T. J. and LIMAYE A., *Physica A*, **339** (2004) 152.
- [13] GRASSELLI *et al.* (*Physica A*, **246** (1997) 301) found, using other protocols, a slight impact of the preparation on the avalanche angles.
- [14] BOUCHAUD J.-P., CATES M. E., PRAKASH J. R. and EDWARDS S. F., *Phys. Rev. Lett.*, **74** (1995) 1982.
- [15] KABLA A. and DEBRÉGEAS G., *Phys. Rev. Lett.*, **92** (2004) 035501.
- [16] JOSSE RAND C., TKACHENKO A., MUETH D. M. and JAEGER H. M., *Phys. Rev. Lett.*, **85** (2000) 3632.
- [17] ASTE T., SAADATFAR M., SAKELLARIOU A. and SENDEN T. J., *Physica A*, **339** (2004) 16.